ACADEMIC PRESS

Available online at www.sciencedirect.com
SCIENCE DIRECT®

Journal of Colloid and Interface Science 262 (2003) 253–262

JOURNAL OF Colloid and Interface Science

www.elsevier.com/locate/jcis

Modeling of spontaneous penetration of viscoelastic fluids and biofluids into capillaries

Konstantin G. Kornev and Alexander V. Neimark *

Center for Modeling and Characterization of Nanoporous Materials, TRI/Princeton, P.O. Box 625, Princeton, NJ 08542, USA

Received 8 August 2002; accepted 14 January 2003

Abstract

A theoretical model was developed to describe the dynamics of spontaneous penetration of viscoelastic fluids into capillaries. The model agrees quantitatively with recent experiments on absorption of droplets of polymer solutions by glass capillaries [A.V. Bazilevsky, K.G. Kornev, A.N. Rozhkov, A.V. Neimark, J. Colloid Interface Sci. (2003)]. The rate of penetration progressively reduces with the increase in fluid elasticity. Analysis revealed two main contributions to the viscoelastic drag of the liquid column: (i) viscous resistance, which is independent of fluid elasticity, and (ii) viscoelastic resistance, known as the Weissenberg effect. We analytically derived an augmented Bosanquet equation for the maximal velocity of penetration by balancing capillary, inertia, and viscoelastic forces. For slow creep of a liquid column, the Lucas–Washburn equation was modified by accounting for the Weissenberg effect. A series of numerical calculations were performed to demonstrate characteristic features of absorption of fluids at different conditions. This article also discusses some problems specific to absorption of biofluids. We show that deformations of cell membranes in the external converging flow may cause their rupture at the pore entrance.

1. Introduction

Numerous applications of porous membranes and substrates in medicine and personal care call for a better understanding of mechanisms of absorption of biofluids by porous materials. However, little is known about the physical mechanisms of absorption of biofluids. The fluid rheology is believed to be crucial, especially at the initial stage of uptake, immediately after a capillary or a porous body is set in contact with the fluid [1]. In the framework of continuum mechanics, one can explain the experimental data on spontaneous absorption of simple viscous fluids by the action of capillary, viscous, and inertial forces. It is assumed that the meniscus forms immediately as the fluid touches the pore wall. The Laplacian capillary pressure associated with the meniscus curvature pulls the liquid into the capillary, while the liquid inertia and friction oppose the movement [2–4]. The simplest, yet instructive model of flow in porous membranes is the flow in straight capillaries (Fig. 1). Despite the obvious shortcomings, it illuminates the role that different forces play in the phenomenon. We use this model to investigate the problem of spontaneous absorption of biofluids carrying polymeric coils or cells, i.e., elastic inclusions.

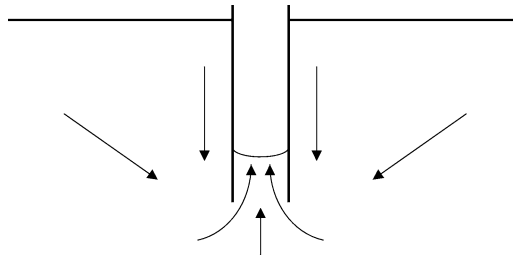

Fig. 1. When a capillary is inserted into a liquid, a sink-like flow is set up at the entrance. The sink strength is controlled by the velocity of the meniscus propagation within the capillary.

It is well documented that biological fluids such as saliva, mucus, and blood are viscoelastic [5–22]. There are different physical origins of biofluid elasticity. Since biofluids are mixtures of biopolymers and emulsions, their viscoelasticity is a result of complex dynamics of biopolymers and cells. Leaving aside a structural complexity of biofluids, we use a phenomenological description. We distinguish two effects associated with deformations of elastic inclusions in shear and extension flows [23,24]. Shear flow deformations cause the so-called Weissenberg effect inherent in the core

* Corresponding author.
E-mail address: aneimark@triprinceton.org (A.V. Neimark).

0021-9797/03/$ – see front matter
doi:10.1016/S0021-9797(03)00072-9

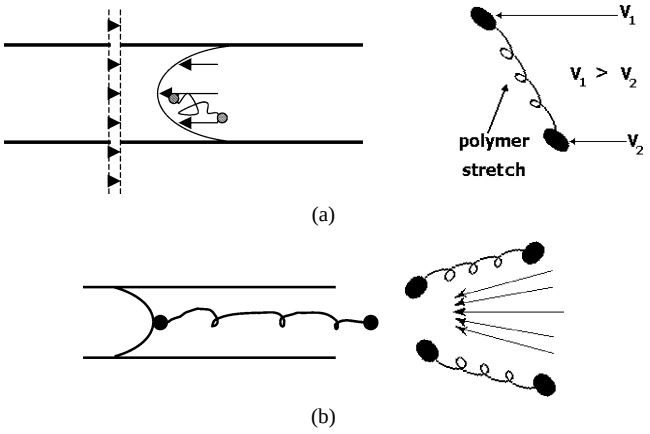

Fig. 2. Mechanisms of elastic reaction of polymer coils/cells responsible for meniscus deceleration. Elastic inclusions are pictured as flexible dumbbells. In a velocity gradient, the dumbbell is transferred with an average velocity and is stretched along with the fluid elements. (a) Weissenberg effect: in the Poiseuillean flow the dumbbell is stretched, giving rise to an extra stress acting normally to the capillary cross section. (b) Spring effect: the meniscus is pulled back due to the dumbbell extension in the sink-like external velocity field. Both effects act simultaneously.

Poiseuillean flow. Extension flow deformations in the converging stream at the pore entrance cause another effect, referred to as the spring effect.

1.1. Weissenberg effect in shear flow

In a Poiseuillean flow with a parabolic velocity profile, elastic inclusions of the fluid are stretched due to the velocity gradients. Their stretching causes a force directed counter to the flow (Fig. 2a). Essentially, the stretching of a viscoelastic fluid gives rise to an extra stress additional to the pressure. This effect, known as the Weissenberg effect [25], causes a reduction of the capillary pressure at the meniscus, leading to a weakening of the driving force.

1.2. Spring effect in extension flow

In a sink-like flow at the capillary inlet, the velocity gradients cause stretching of elastic inclusions also. However, the mechanism explaining the friction drag is different from the Weissenberg effect. Imagine a spring (Fig. 2b), of which one end is attached to the meniscus, and the other is kept outside the capillary. As the meniscus propagates inside the capillary, the spring is strained and pulls the meniscus backward. The effect may be significant at the initial instants of penetration, within the time intervals comparable to the characteristic time of relaxation of elastic inclusions.

In this article, we focus on the physical mechanisms of absorption of viscoelastic fluids by capillaries. We restrict ourselves to sufficiently wide pores, for which a continual hydrodynamic theory can be applied. In Section 2 we derive the basic governing equation taking into account the Weissenberg and spring effects (Appendix A contains the mathematical details). An asymptotic analysis of the model illustrates the characteristic features of some limiting regimes of flow. In Section 3, we numerically study two problems: penetration of liquid into capillaries without gravity and capillary rise. In Section 4, we analyze the spontaneous absorption of biofluids and propose scaling arguments to estimate the flow-induced interactions of cells with submicrometer capillaries. We show that the capillary pressure may rupture the cell if the pore size is comparable to the cell radius or smaller. The rupture occurs at the pore entrance due to the hydrodynamic stretching of the cells. Section 5 summarizes the results.

2. The model and analysis of limiting cases

A schematic picture of the absorption experiment is presented in Fig. 1. An empty capillary is submerged into a liquid and, as soon as the capillary touches the liquid surface, the liquid begins to penetrate inside the capillary.

In capillaries whose radius is greater than the characteristic coil/cell size, the fluid flow may be considered within the framework of continuum hydrodynamics. The driving force of the process is not the pressure gradient, but the wetting force acting at the contact line. Therewith, the contact line drags the meniscus, and the flow pattern at the vicinity of the meniscus is a plug-like flow with an almost constant velocity profile. The development of a boundary layer and the transition from the plug-like flow to the Poiseuillean flow are beyond the scope of this article. A non-Newtonian constitutive equation accounts for the fluid structural complexity. We use the upper convected Maxwell model for description of viscoelastic fluids [24,28]. The Maxwell model is suitable for fluids displaying an elastic response within short time intervals and behaving as viscous fluids at longer times [13,28–33]. The elastic response is characterized by the relaxation time $\lambda = \eta/G$, which is the ratio of fluid viscosity η to the elastic modulus G of the fluid.

2.1. Basic equation

Accounting for the Maxwellian rheology, the equation of meniscus motion through capillary of radius R is written as

$$\rho R^2 d\big((x + cR)dx/dt\big)\big/dt + 8\eta x\, dx/dt + (16\lambda\eta)(dx/dt)^2 + R^2\mathcal{F}(dx/dt, \lambda, \eta) - 2\sigma R\cos\theta + \rho g x R^2 = 0. \quad (1)$$

The details of derivation of the model for viscous fluids can be found in [34]; the terms specific for viscoelastic fluids are derived in Appendix A. In Eq. (1), x is the meniscus coordinate, t is the time, and ρ is the density. The first term in Eq. (1) is the inertial force. Parameter c accounts for the apparent mass contribution due to the external flow and is of the order of one [34–36]. The second term is the friction force due to the fluid viscosity. The third term expresses the Weissenberg effect. The fourth term accounts for the spring

effect of flow at the pore entrance causing an extra pressure $\mathcal{F}(dx/dt, \lambda, \eta)$. The fifth term is the capillary driving force, σ is the surface tension, and θ is the contact angle. The last term is the gravitational force. Taking $c = 0$, $\lambda = 0$, and $\mathcal{F}(dx/dt, \lambda, \eta) = 0$, we arrive at the Bosanquet equation [4]. For simple viscous fluids, the so-called Bosanquet velocity [4], given by

$$U_B = \sqrt{2\sigma \cos\theta/\rho R}, \tag{2}$$

serves as a benchmark for the magnitude of meniscus velocity. It appears as a natural initial condition for the Bosanquet equation [4]. Different applications of the Bosanquet equation and Eq. (2) for analyses of fluid penetration were considered in Refs. [37–39], and, in great detail, in Refs. [36,40,41]. The Bosanquet velocity U_B can be obtained by writing the momentum balance for the moving column neglecting viscosity and external hydrodynamics [41]. Most recently, the role of the Bosanquet velocity as an upper estimate of the rate of absorption in the very beginning of penetration from a bulk liquid reservoir was revisited in Refs. [34,36,42].

Mathematically, the Bosanquet velocity is a singular point of the Bosanquet equation as x and t tend to zero [34]. The ansatz $x \sim U_B t + O(t^2)$ selects a unique initial condition [40], which provides for a consistency of the corresponding Cauchy problem. If one assumes a "natural" initial condition $dx/dt = 0$ at $t = 0$, the account for a finite apparent mass is necessary for the problem regularization. Starting with zeroth velocity, the meniscus accelerates and attains a maximum velocity within a short interval. As shown below, a numeric investigation of the problem confirms the statement that the Bosanquet velocity gives an accurate upper estimate of the initial velocity of meniscus penetration.

2.2. How does the viscoelasticity change the Bosanquet velocity?

Consider the initial stage of fluid penetration, during which the meniscus travels only a few capillary diameters. We augment the Bosanquet analysis [4] to include the effect of fluid elasticity. The Poiseuillean friction is not important in the limit $x \to 0$. As shown in Appendix A, in the asymptotic case of elasticity domination, $R/\lambda \ll dx/dt$, the function $\mathcal{F}(dx/dt, \lambda, \eta)$ behaves as $\mathcal{F}(dx/dt, \lambda, \eta) \propto (\eta/\lambda)(\lambda[dx/dt]/R)^{4/3}$. Neglecting the effect of apparent mass and the weight of the liquid column, Eq. (1) is reduced to

$$\rho R^2 d(x\,dx/dt)/dt + R^2 c_{\mathrm{VE}}(\eta/\lambda)\big(\lambda[dx/dt]/R\big)^{4/3} + (16\lambda\eta)(dx/dt)^2 - 2\sigma R\cos\theta = 0, \tag{3}$$

where $c_{\mathrm{VE}} = \pi 3^{5/6} 2^{2/3}/(18\Gamma(2/3)) \approx 0.511$. Looking for an asymptotic solution in the form $dx/dt \sim U_{\mathrm{VE}} + \omega_1 t + \cdots$, we come to the equation for U_{VE}:

$$\rho R^2 U_{\mathrm{VE}}^2 + R^2 c_{\mathrm{VE}}(\eta/\lambda)(\lambda U_{\mathrm{VE}}/R)^{4/3} + (16\lambda\eta)U_{\mathrm{VE}}^2 - 2\sigma R\cos\theta = 0. \tag{4}$$

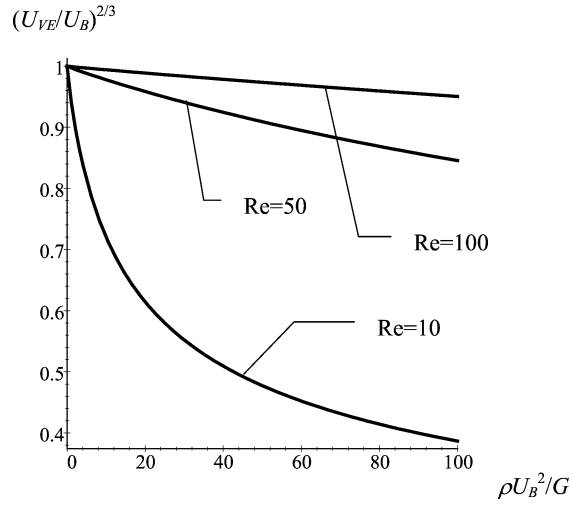

Fig. 3. Dimensionless velocity for viscoelastic fluids as a function of the ratio of kinetic energy to elastic energy.

Using the substitution $U_{\mathrm{VE}}^{2/3} = U_B^{2/3}\zeta$, we rewrite Eq. (4) as

$$(1 + 16Wi/Re)\zeta^3 + c_{\mathrm{VE}}\frac{Wi^{1/3}}{Re}\zeta^2 - 1 = 0, \tag{5}$$

where the Reynolds number is defined as

$$Re = \frac{\rho R U_B}{\eta},$$

and the Weissenberg number, which shows a relation between the inertial and elastic forces, is defined as

$$Wi = \frac{\lambda U_B}{R} = \frac{\rho U_B^2}{G}\frac{1}{Re}. \tag{6}$$

In Fig. 3, we plot the solution of Eq. (5) for different Reynolds numbers.

While the parameter $1/Re$ is small, there are different flow regimes depending on the magnitude of the Weissenberg number.

2.2.1. Small $1/Re$ and Wi

When the Weissenberg number is small, we have an asymptotic solution of Eq. (5) as

$$\zeta = 1 - \left(\frac{\rho U_B^2}{G}\right)^{1/3}\frac{c_{\mathrm{VE}}}{3Re^{4/3}} + \cdots,$$

or, in the dimensional form,

$$U_{\mathrm{VE}} = U_B\left(1 - \left(\frac{\rho U_B^2}{G}\right)^{1/3}\frac{c_{\mathrm{VE}}}{2Re^{4/3}} + \cdots\right). \tag{7}$$

Equation (7) is a suitable estimate of the initial velocity of fluid uptake for the regimes in which the spring effect of the external flow dominates the Weissenberg effect.

2.2.2. Small $1/Re$ and large Wi

There is another asymptote, when the Weissenberg number is large. In such a case, the Weissenberg effect prevails over the spring effect, so that the external flow does not play

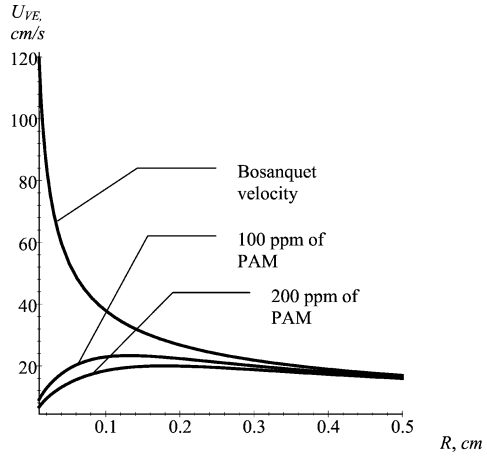

Fig. 4. U_{VE} given by Eq. (8) as a function of capillary radius for aqueous solutions of polyacrylamide (PAM). $\eta = 4$ mPa s, $\lambda = 0.027$ s for 100 ppm and $\lambda = 0.05$ for 200 ppm solutions of PAM. $\sigma = 71$ mN/m, $\theta = 0$ for both solutions [1].

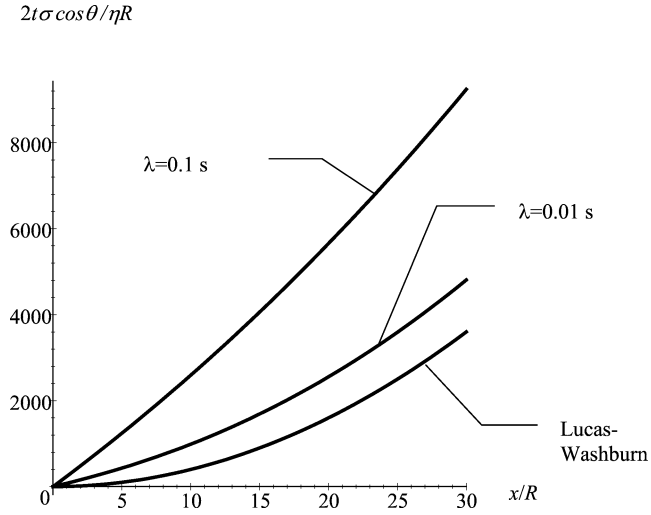

Fig. 5. Noninertial motion of meniscus of viscoelastic and viscous fluids. $\eta = 4$ mPa s, $\sigma = 71$ mN/m, $\theta = 0$.

a significant role. The characteristic velocity is given by

$$U_{\mathrm{VE}} = U_B/\sqrt{1 + 16\eta\lambda/\rho R^2} = \sqrt{\frac{2\sigma R\cos\theta}{\rho R^2 + 16\eta\lambda}}. \tag{8}$$

In the preceding paper [1], we demonstrated experimentally that the modified Bosanquet velocity, Eq. (8), quantitatively describes the rate of penetration of droplets of polymer solutions into capillaries (see Table 1 in Ref. [1]). Equation (8) gives a nonmonotonous dependence of the velocity U_{VE} on the capillary radius. Remarkably, the velocity U_{VE} attains a maximum at the radius $R_{\mathrm{VE}} = 4\sqrt{\lambda\eta/\rho}$, which is independent of the wetting properties of liquids. If the pore radius is smaller than R_{VE}, the velocity decreases due to the Weissenberg effect. If the radius is greater than R_{VE}, the velocity decreases because of a reduction of the driving capillary pressure. As shown in Fig. 4, the difference between absorption rates of simple and viscoelastic fluids is significant. As a typical example, we have presented the data for aqueous solutions of polyacrylamide (PAM). This well-documented system was used to model the blood rheology [21,22,43].

2.3. Noninertial flow, or the Lucas–Washburn limit

At the intermediate time scale when the entrance effects can be neglected and the inertial forces are dominated by the friction forces, Eq. (1) can be rewritten as

$$8\eta x\,dx/dt + (16\lambda\eta)(dx/dt)^2 - 2\sigma R\cos\theta + \rho g x R^2 = 0. \tag{9}$$

Equation (9) admits the exact integration, yet the form of the integral is complex. Ignoring gravity, the solution reduces to

$$\frac{t - t_0}{\eta R}\sigma\cos\theta = \left[\frac{x^2}{R^2} + \frac{x}{R}\sqrt{\frac{x^2}{R^2} + \frac{2\sigma\lambda\cos\theta}{\eta R}}\right] + \frac{2\sigma\lambda\cos\theta}{\eta R}\log\left(\frac{x}{R} + \sqrt{\frac{x^2}{R^2} + \frac{2\sigma\lambda\cos\theta}{\eta R}}\right), \tag{10}$$

where t_0 is an integration constant. Equation (10) plays the same role as the Lucas–Washburn equation of front propagation in the case of viscous fluids [44,45]. The difference between Eq. (10) and the Lucas–Washburn equation, $(t - t_0)\sigma\cos\theta/\eta R = 2x^2/R^2$, is shown in Fig. 5. There is no doubt that the Weissenberg effect is significant and distinguishable from the effect of Poiseuillean friction. Thus, the method of dynamic absorption suggested in the preceding article [1] is quite promising not only as a mean for characterization of fluid/wall interactions, but also as a tool for studying the fluid rheology. The elastic modulus $G = \eta/\lambda$ can be found from an analysis of the meniscus propagation, provided that other parameters are determined independently. Below, we numerically investigate the problem of the meniscus motion to find the distance range where Eq. (10) is applicable.

3. Numerical analysis of the model

3.1. On applicability of the approximation of noninertial flow: no gravity

From the asymptotic analysis of the model, we concluded that the spring effect plays a minor role for most cases under consideration. Hence, the fourth term in Eq. (1) may be neglected and the equation takes on the form

$$\rho R^2 d\big((x + cR)dx/dt\big)\big/dt + 8\eta x\,dx/dt + (16\lambda\eta)(dx/dt)^2 - 2\sigma R\cos\theta = 0. \tag{11}$$

This equation is subjected to "natural" initial conditions

$$x = 0, \qquad dx/dt = 0, \quad \text{at } t = 0.$$

It is convenient to rewrite the equation in the dimensionless variables by introducing the characteristic time $\tau =$

$\sqrt{\rho R^3/2\sigma\cos\theta}$ and taking the radius of capillary as a characteristic length scale. Within this normalization, Eq. (11) takes on the form

$$d\big((H+c)dH/dT\big)\big/dT + \Omega\, dH/dT(H + De\, dH/dT) = 1, \qquad (12)$$

where

$$H = x/R, \qquad T = t/\tau, \qquad \Omega = \frac{8\tau\eta}{\rho R^2}, \qquad De = 2\lambda/\tau.$$

The parameter Ω characterizes the magnitude of the viscous forces, and the Deborah number *De*, the magnitude of the elastic forces, as compared with the driving force of penetration.

The term responsible for the viscous drag is proportional to the distance traveled by the meniscus, $\Omega H(dH/dT)$. This term may be very small at the initial instance of time compared with the Weissenberg term which is independent of the distance, $\Omega De(dH/dT)^2$. Hence, the elastic forces resist the motion effectively even at the very beginning of penetration, and the greater the relaxation time, the stronger the effect.

In calculations, we set $c = 1$ as a reasonable approximation of experimental situations [36]. The contact angle is assumed to be zero. All physical parameters correspond to those of water:

$$\eta = 1\ \text{mPa s}, \qquad \sigma = 72\ \text{mN/m}, \qquad 2R = 0.65\ \text{mm},$$
$$\rho = 1000\ \text{kg/m}^3.$$

We vary only the relaxation time λ to display the effect of fluid elasticity. As a typical example, in Fig. 6, we plot the meniscus velocity as a function of the traveled distance. The velocity takes its maximal value when the meniscus had traveled few capillary diameters. The maximums are smaller than U_B (viscous fluids) and U_{VE} (viscoelastic fluids), but the differences are insignificant. Therefore, the characteristic velocities U_B and U_{VE} provide a correct estimate for the initial velocity.

The asymptotic formula (10) works quite well: the greater the relaxation time, the better the approximation. For a particular case of aqueous solutions of PAM, whenever the meniscus travels about 10 diameters, the approximate formula is applicable for concentrations greater than 100 ppm ($\lambda > 0.03$, see Fig. 7 in Ref. [1]).

3.2. Penetration of droplets into capillaries

In the preceding article [1], we applied Eq. (11) to predict the rate of absorption of droplets of polymer solutions into capillaries. Equation (11) was modified to account for the gravity and the varying size of a penetrating droplet. It was shown that the model predicts the rate of absorption fairly well without any adjustable parameters (see Fig. 11 in Ref. [1]).

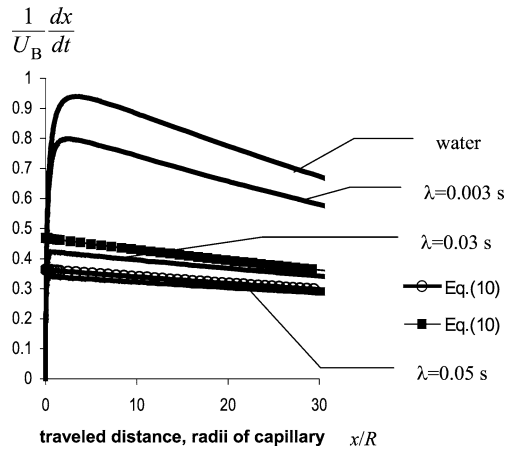

Fig. 6. Meniscus velocity normalized by the Bosanquet velocity as a function of the traveled distance measured in radii of the capillary. Two asymptotes are calculated by Eq. (10) with $\lambda = 0.03$ s and $\lambda = 0.05$ s, respectively.

3.3. Capillary rise

Considering the problem of capillary rise, we also neglect the fourth term in Eq. (1). The natural length scale in this problem is the Jurin length, $\ell_{\text{cap}} = 2\sigma\cos\theta/\rho g R$, i.e., the height of the liquid column under equilibrium conditions. The time $\tau_r = \sqrt{\ell_{\text{cap}}/g}$ of free fall of liquid column of length ℓ_{cap} serves as a characteristic time. Taking this normalization, we rewrite Eq. (1) in dimensionless form as

$$d\big((H+\alpha)dH/dT\big)\big/dT + \Omega_r\, dH/dT(H + De_r\, dH/dT) = 1 - H, \qquad (13)$$

where

$$H = x/\ell_{\text{cap}}, \qquad T = t/\tau_r, \qquad \alpha = cR/\ell_{\text{cap}},$$
$$\Omega_r = 8\eta\ell_{\text{cap}}/(\rho R^2 g\tau_r), \qquad De_r = 2\lambda/\tau_r.$$

Due to the difference in the time scales, the Deborah number De_r is different from that introduced in Eq. (12). It characterizes a relation between the effects of elasticity and inertia. For a quantitative analysis of the elastic effect, we plot in Fig. 7a the column height measured in the Jurin length as a function of the dimensionless time, scaled by τ_r. All physical parameters correspond to water.

For viscoelastic fluids, the time needed for the liquid column to achieve a certain vicinity of the limiting Jurin height increases drastically as the relaxation time increases. The effect is apparent in Fig. 7b where the meniscus velocity is shown as a function of the traveled distance. While gravity is insignificant at the beginning when the meniscus accelerates to its maximal velocity, the gravitation-induced deceleration prevails just after this maximal point (Fig. 7c). Figure 7c shows that a significant decrease in the rate of absorption due to gravity can be expected only for viscoelastic fluids with a small relaxation time: the greater the relaxation time, the smaller the effect of gravity.

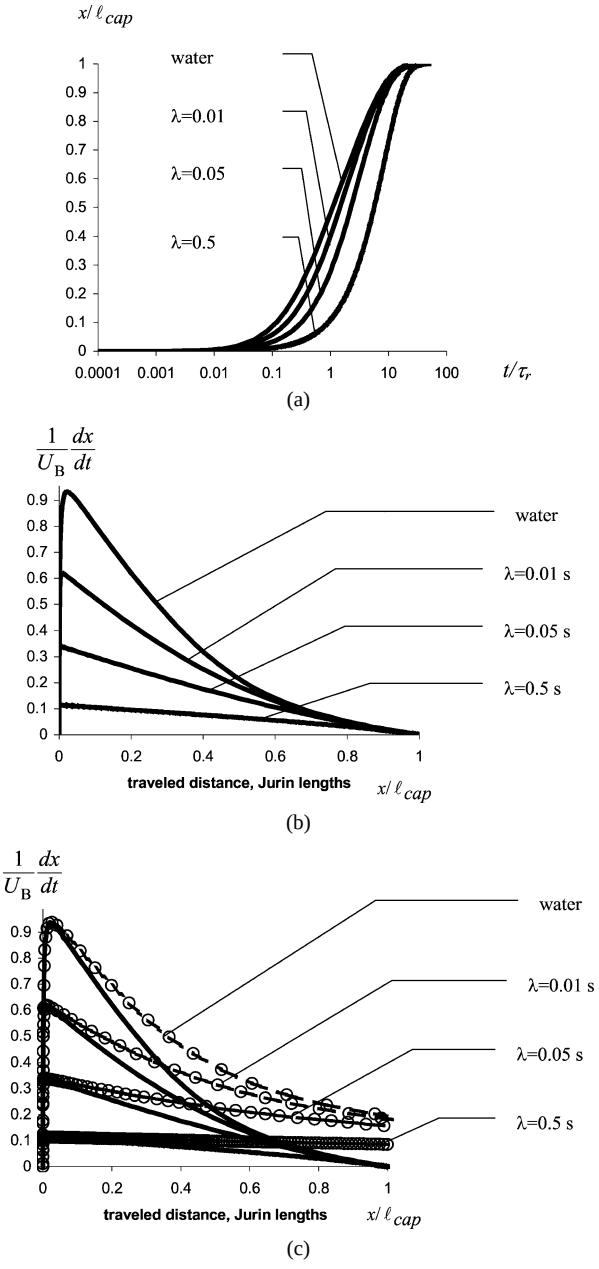

Fig. 7. Dynamics of capillary rise of water and viscoelastic Maxwellian fluids. (a) Length of liquid column as a function of time; (b) meniscus velocity as a function of traveled distance; (c) same as (b) and a series of curves corresponding to "no gravity" conditions.

4. Note on the size effects for fluids containing biocells

The problem of spontaneous absorption is related to a well-known test of blood filterability [26,27,46,47]. In the filterability measurements, a given biofluid is forced to move through a filter with micrometer-size pores. Mechanical properties of the cells, in particular the cell's ability to pass through the filter, are examined. The breakthrough time is measured and compared with the data on the reference blood to reveal the abnormal cell behavior. The existing theory

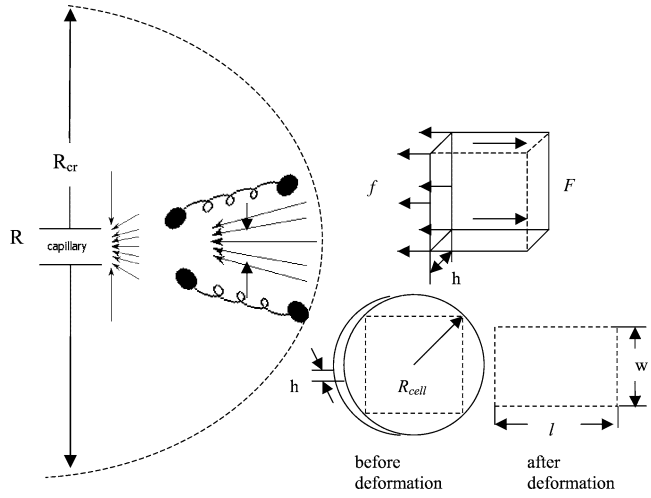

Fig. 8. Inside the semisphere of radius R_{cr} the biocells are stretched, while outside this region their shape is almost unperturbed.

of the method is based on an analysis of the cell motion inside a capillary [48–52]. However, the fluid filterability is also limited by the hydrodynamic separation of polymeric coils/cells at the pore entrance due to the spring effect. This effect is hindered in the regime of forced filtration; however, it may be significant in the case of spontaneous absorption. Below, we analyze this effect by using simple scaling arguments [53].

4.1. Biocells in a sink-like flow

Consider a dilute solution of cells. The cell is modeled as a liquid-filled membrane with the surface elastic modulus E [54,55]. At the pore entrance, the external flow is convergent and can be modeled by a sink-like pattern (Fig. 8). Thus, at distance r from the pore entrance the velocity υ_r and its gradient $\Gamma = -d\upsilon_r/dr$ are given by

$$\upsilon_r = \frac{1}{2}\frac{R^2}{r^2}U, \qquad \Gamma(r) = -\frac{d\upsilon_r}{dr} = \frac{R^2}{r^3}U. \tag{14}$$

Here U is the meniscus velocity. Let us assume a boundary $r = R_{cr}$, outside which the cell in solution moves toward the capillary by keeping its shape almost unperturbed. At the boundary $r = R_{cr}$, the tensile force due to the velocity gradient is approximately equal to the elastic force of the cell membrane (Fig. 8). This schematic picture of cell/flow interaction allows us to exhibit the effect of size of a capillary on the cell stability against rupture. To estimate the critical radius, we model the cell as a square parallelogram of thickness h, the face side being of the order of the radius R_{cell} of the discoidal cell in its unperturbed state (Fig. 8). Assuming that the cell is stretched as a rectangular strip of constant thickness h [56,57]. For the elastic stress, we have the following estimate: $F/(hw) \approx E(l - R_{cell})/R_{cell}$. On the other side, the tensile stress due to the flow is assessed as $f/(hw) = \eta\Gamma(r)lw/(hw)$. Equating these stresses at the

boundary $r = R_{cr}$, we get

$$\eta\Gamma|_{r=R_{cr}}\frac{l}{h} \approx \frac{E(l - R_{cell})}{R_{cell}}. \tag{15}$$

Here, η is the fluid viscosity. Substituting Eq. (14) in Eq. (15), and setting $l \approx (1 + \varepsilon)R_{cell}$, $\varepsilon \ll 1$, we get an estimate of the critical distance as

$$R_{cr} = \left(\frac{\eta R_{cell} R^2 U}{E\varepsilon h}\right)^{1/3}. \tag{16}$$

Substituting Eq. (2) into Eq. (16), we come to the relationship

$$R_{cr} = \left(\frac{\eta R_{cell} R^{3/2}\sqrt{2\sigma\cos\theta}}{E\varepsilon h\sqrt{\rho}}\right)^{1/3}. \tag{17}$$

For a crude yet instructive estimate, we take the typical parameters for red cells and blood as [54,56,57]

$R_{cell} \approx 10$ μm, $E \approx 10^3$ Pa, $\sigma \approx 50$ mN/m,
$\eta \approx 1$ mPa s, $\rho \approx 1000$ kg/m^3,
$\theta \approx 0$, $h \approx 0.01$ μm.

Then $R_{cr} \approx 0.2\sqrt{R}/\sqrt[3]{\varepsilon}$ cm. For 10-μm capillaries and $\varepsilon = 0.1$, the critical radius is about one order of magnitude greater than the pore radius. As shown above, the Bosanquet-like regime of spontaneous absorption lasts about $\approx R/U$. This time interval is small, yet sufficient to produce giant stresses which, most likely, the cell membrane cannot withstand. For example, red blood cells are able to sustain only about 140% extension before the rupture [54].

Thus, the scaling analysis shows that the small-sized capillaries are unsuitable for testing cell deformability in the spontaneous mode of absorption. The use of porous permeable substrates instead of capillaries is questionable also, though the flow pattern at the membrane surface is different. It is worth noting that substrates for which the characteristic distance between pores is sufficiently larger than the pore radius could be appropriate as efficient wound covers. Indeed, cell membranes, which are ruptured in the suction flow, would coat the pore walls, promoting the subsequent platelet adherence [58]. The effect of the cell rupture in the process of spontaneous absorption is worth further studies.

5. Conclusions

The problem of spontaneous penetration of viscoelastic fluids and biofluids into capillaries has been analyzed. The hydrodynamic theory of absorption of viscoelastic Maxwellian fluids is applied for the description of meniscus propagation. We show that the absorption kinetics can be quantitatively described by Eq. (1), a generalized Lucas–Washburn equation. This equation accounts for acceleration of the flow caused by the Laplace pressure, inertia of the fluid column, gravity, viscous friction due to the Poiseuillean flow inside the capillary, the spring effect of stretching of elastic inclusions in the external convergent flow, and the Weissenberg effect of stretching of elastic inclusions in the internal Poiseuillean flow. Commonly, the restoring force due to the spring effect is much smaller than that due to the Weissenberg effect.

The Weissenberg effect gives rise to a reduction of the driving pressure drop, which, in turn, results in the hindrance of absorbency. The effect is pronounced in the case of negligible gravity, for which an analysis of the limiting cases is analytically performed. At the initial instance of time when the flow is controlled by inertial, capillary, and elastic forces, the spring and Weissenberg effects can be distinguished. An analysis becomes evident if the apparent mass of the liquid column is neglected. Therewith, the initial velocity of the meniscus propagation is a constant, which serves as an estimate of the maximum rate of absorption. For small Weissenberg numbers defined by Eq. (6), the spring effect dominates the Weissenberg one. The maximum velocity expressed by Eq. (7) differs slightly from the Bosanquet value. As the Weissenberg number increases, thus manifesting the fluid elasticity, the Weissenberg effect prevails over the spring effect and the maximum velocity is estimated by Eq. (8). As shown by solving the problem (11), (12) numerically, this estimate is quite accurate. The maximal achievable velocity of the meniscus depends on the radius of capillary nonmonotonously; there is a capillary, for which the velocity is maximal, $R_{VE} = 4\sqrt{\lambda\eta/\rho}$. This estimate determines the size of the most efficient capillary for fluid absorption.

An asymptote for the slow noninertial motion of meniscus, similar to the Lucas–Washburn equation for viscous fluids, is found for viscoelastic fluids. It is shown numerically that the asymptotic formula (10) works well for distances of penetration greater than about 10 capillary diameters. This formula operates with the elastic modulus of the fluid. We conclude that the elastic modulus of biofluids can be estimated from the absorption experiment, provided that the surface tension and the contact angle are known, or measured independently.

We showed that the stretching in the converging flow might lead to the rupture of cell membranes in the process of biofluid absorption by fine capillaries. This effect is likely to be more important than the pore clogging by deformed cells. A cell can be delivered safely only to a pore whose size is greater than the cell diameter. The analysis of biofluid absorption by capillaries and porous substrates may have practical implications in health care and medicine, ranging from blood tests to wound treatment.

The model developed in this article was used in the preceding article [1] for the interpretation of experimental data on spontaneous penetration of droplets of polymer solutions into capillaries. It was shown that the model describes the experiments without any adjustable parameters involved and gives correct relations between the rate of penetration and rheological parameters.

Acknowledgments

The work was supported by the Johnson & Johnson Focused Giving Program and a group of TRI/Princeton corporate members.

Appendix A

The derivation of Eq. (1) for viscous fluids can be found in Refs. [34,45]. Therefore, we focus on the derivation of the third and fourth terms in Eq. (1).

For viscoelastic fluid satisfying the upper convected Maxwell model, the relation between the stress tensor and strain rate tensor is given by [24]

$$\Sigma + \lambda \frac{\delta \Sigma}{\delta t} = 2\eta D, \tag{A.1}$$

where $D = (\nabla \mathbf{u} + \nabla \mathbf{u}^{\mathrm{T}})/2$ is the strain rate tensor, with the index T denoting the transpose operator, Σ is the stress tensor, λ is the relaxation time, η is the shearing viscosity, and $\delta/\delta t$ is the convected derivative,

$$\frac{\delta \Sigma}{\delta t} = \frac{\partial \Sigma}{\partial t} + \nabla \cdot (\mathbf{u}\Sigma) - L\Sigma - \Sigma L^{\mathrm{T}}, \tag{A.2}$$

where $L = \nabla \mathbf{u}^{\mathrm{T}}$ is the velocity gradient tensor. This derivative takes into account the kinematics of stretching of polymer chains/biocells in the field of the given velocity gradient. Considering the polymer chain/biocell as a dumbbell, the physical meaning of different terms in (A.2) can be elucidated as a combination of advection and additional stretching [24,28]. Setting the relaxation time to be zero, we arrive at the ordinary Navier–Stokes equation for viscous fluids.

Elasticity effects, wall friction

For unidirectional flows of viscoelastic fluid, the Poiseuillean velocity distribution holds, which can be checked by direct substitution of the velocity distribution into the momentum equation. Assuming also that the flow is driven by the pressure gradient, one can be convinced that the extra stress is uniform over the capillary, and has the form

$$\Sigma_{zz} = 2\eta\lambda\left(\frac{du_z}{dR}\right)^2.$$

Substituting the Poiseuillean profile and averaging it over the capillary cross section, we arrive at the third term in Eq. (1).

Entrance effect in the case of elastic fluid

The entrance effect results in (i) the changes of apparent mass of a liquid column and (ii) the effective column resistance. Both corrections depend on the flow pattern at the capillary brim. Two types of flow patterns just beneath the capillary inlet have been discussed in the literature: the vortex growth regime and the divergent flow regime (see Refs. [23,59,60] for review). In the vortex growth regime, the moving fluid is confined to the slender conical region, with the fluid outside forming two toroidal vortices. Under some flow conditions, the half-angle $\Phi/2$ of the cone was found to be about $\Phi/2 = \pi/12 = 15^\circ$ [59]. In the limiting case, the divergent flow regime, the sink-like flow pattern spreads over the whole domain, $\Phi = 2\pi$.

In the derivation of Eq. (1) we use an approximation of a sink-like flow at the capillary entrance [35]. Therewith, the apparent mass is the same as that calculated in Ref. [35]. However, the effect of flow resistance due to viscosity and elasticity deserves special attention. In sink-like flow, there are three nonzero components of the stress tensor, all of which are diagonal [24,28]. The upper convected Maxwell model is reduced to two equations of the form [61,62]

$$\Sigma_{RR} + \lambda\left(-\frac{Q}{r^2}\frac{d\Sigma_{RR}}{dr} - \frac{4Q}{r^3}\Sigma_{RR}\right) = \frac{4\eta}{r^3}Q, \tag{A.3}$$

$$\Sigma_{\theta\theta} + \lambda\left(-\frac{Q}{r^2}\frac{d\Sigma_{\theta\theta}}{dr} + \frac{2Q}{r^3}\Sigma_{\theta\theta}\right) = -\frac{2\eta}{r^3}Q, \tag{A.4}$$

where $Q = (R^2 dx/dt)/[2(1-\cos(\Phi/2))]^2$ is the flow rate. Between the two components of the stress tensor the relation $\Sigma_{\theta\theta} = \Sigma_{\varphi\varphi}$ holds. All components must vanish at infinity. The solutions to these equations are [61]

$$\Sigma_{RR} = \frac{4\eta}{3\lambda} J\left(\frac{R^3}{3\lambda Q}, \frac{4}{3}\right), \tag{A.5}$$

$$\Sigma_{\theta\theta} = \Sigma_{\varphi\varphi} = -\frac{2\eta}{3\lambda} J\left(\frac{R^3}{3\lambda Q}, -\frac{2}{3}\right), \tag{A.6}$$

where

$$J(z,m) = e^z z^{-m} \int_z^\infty e^{-y} y^{m-1}\, dy. \tag{A.7}$$

The momentum balance gives an additional equation for the thrust T as

$$T \approx 2\int_{r_*}^\infty (\Sigma_{RR} - \Sigma_{\theta\theta})\frac{dr}{r}, \tag{A.8}$$

where $r_* = R/\sin(\Phi/2)$.

Consider two limiting cases.

Viscosity-dominated regime. The following inequality $r_*^3/\lambda Q \gg 1$ holds, and we can use the asymptotic values of integrals, namely,

$$J(z,m) = e^z z^{-m} \int_z^\infty e^{-y} y^{m-1}\, dy \approx 1/z, \quad z \to \infty. \tag{A.9}$$

Then Eq. (A.8) takes the form

$$2\int_{r_*}^\infty (\Sigma_{RR} - \Sigma_{\theta\theta})\frac{dR}{R} \approx \frac{4\eta Q}{r_*^3}. \tag{A.10}$$

Elasticity-dominated regime [62]. The inequality $r_*^3/\lambda Q \ll 1$ holds, and we can use the asymptotic value of the

integrals

$$J(z,m) = e^z z^{-m} \int_z^\infty e^{-y} y^{m-1}\,dy \approx \Gamma(m)/z^m,$$
$$z \to 0,\ m > 0,$$
$$J(z,m) = e^z z^{-m} \int_z^\infty e^{-y} y^{m-1}\,dy \approx -1/m,$$
$$z \to 0,\ m < 0. \tag{A.11}$$

Then we get the formula $\mathcal{F}(dx/dt,\lambda,\eta) \approx c_{\mathrm{VE}}(\eta/\lambda)(\lambda[dx/dt]/R)^{4/3}$ with the prefactor

$$c_{\mathrm{VE}} = \pi 3^{5/6} 2^{2/3} \big/ \big(18\Gamma(2/3)\big) \approx 0.511.$$

The viscous dissipation at the inlet

It is instructive to estimate the tensile force caused by friction outside the pore in the case of viscous fluid. Assuming that the flow is a converging radial stream, and the fluid is incompressible, we have the following velocity distribution in the lower semispace $u_R = Q/R^2$. The latter implies that the shearing deformations are entirely absent. In other words, there are only extensional deformations with the diagonal rate-of-deformation tensor e_{ij}. In the spherical coordinate system, the principal components of the latter are $e_{rr} = du_r/dr$, $e_{\theta\theta} = e_{\varphi\varphi} = -(1/2)du_r/dr$. The viscous dissipation associated with this velocity field is

$$W \approx \int_R^\infty 2\eta e_{ij} e_{ij} 2\pi r^2\,dr = \int_R^\infty 3\eta \frac{R^4}{r^6}\left(\frac{dx}{dt}\right)^2 2\pi r^2\,dr$$
$$= 2\pi\eta R\left(\frac{dx}{dt}\right)^2. \tag{A.12}$$

Therefore, in addition to Poiseuillean friction force $\pi R^2\rho(8\eta/\rho R^2)x\,dx/dt$, we get the term $\pi R^2\rho(2\eta/R\rho)\,dx/dt$ which is exactly (A.10). This force dominates the Poiseuillean force at the initial instants of time, while at the late stage of penetration, when the column passes a few diameters of capillary, this tensile force becomes insignificant.

References

[1] A.V. Bazilevsky, K.G. Kornev, A.N. Rozhkov, A.V. Neimark, J. Colloid Interface Sci. 261 (2003) 16.
[2] R. Lucas, Kolloid Z. 23 (1918) 15.
[3] E.W. Washburn, Phys. Rev. 17 (1921) 273.
[4] C.H. Bosanquet, Philos. Mag. 45 (6) (1923) 525.
[5] R. Adell, R. Skalak, P. Branemar, Blut 21 (1970) 91.
[6] I. Anadere, H. Chmiel, W. Laschner, Biorheology 16 (1979) 179.
[7] S. Anand, S.K. Guha, Med. Biol. Eng. Comput. 16 (1978) 256.
[8] J.P. Barras, J. Blattner, VASA J. Vasc. Dis. 14 (1985) 216.
[9] M.L. Chatkoff, Gynecol. Invest. 6 (1975) 105.
[10] S. Chien, R.G. King, R. Skalak, S. Usami, A.L. Copley, Biorheology 12 (1975) 341.
[11] G.R. Cokelet, Annu. Rev. Physiol. 42 (1980) 311.
[12] P.F. Dunn, B.F. Picologlou, Biorheology 13 (1976) 379.
[13] A.M. Giordano, D. Holsclaw, M. Litt, Am. Rev. Respir. Dis. 118 (1978) 245.
[14] J. Gomez, G.B. Thurston, Biorheology 23 (1986) 298.
[15] J. Mauss, J. Pradere, J. Biophys. Med. Nucl. 5 (1981) 185.
[16] D.E. McMillan, N. Utterback, Biorheology 17 (1980) 343.
[17] B.K. Rubin, O. Ramirez, M. King, Chest 101 (1992) 1080.
[18] R. Skalak, N. Ozkaya, T.C. Skalak, Annu. Rev. Fluid Mech. 21 (1989) 167.
[19] G.B. Thurston, Biophys. J. 12 (1972) 1205.
[20] M. Pohl, O. Samba, M.O. Wendt, G. Vlastos, Int. J. Artif. Organs 21 (1998) 107.
[21] G. Vlastos, D. Lerche, B. Koch, Biorheology 34 (1997) 19.
[22] D. Lerche, G. Vlastos, B. Koch, M. Pohl, K. Affeld, J. Phys. III 3 (1993) 1283.
[23] S. Middleman, Fundamentals of Polymer Processing, McGraw–Hill, New York, 1977.
[24] R.B. Bird, R.C. Armstrong, O. Hassanger, Fluid Mechanics, Vol. 1: Dynamics of Polymeric Liquids, Wiley, New York, 1987.
[25] K. Weissenberg, Nature 159 (1947) 310.
[26] G.B. Nash, Biorheology 27 (1990) 873.
[27] S.A. Evans, R. Adams, G.B. Nash, Biorheology 36 (1999) 453.
[28] R.G. Larson, The Structure and Rheology of Complex Fluids, Oxford Univ. Press, New York, 1999.
[29] G.W. ScottBlair, J. Burnett, Kolloid Z. 168 (1960) 98.
[30] M. Litt, Bull. Physio-Pathol. Respir. 9 (1973) 33.
[31] D.P. Wolf, M.A. Khan, M. Litt, Fertil. Steril. 26 (1975) 197.
[32] P.Y. Tam, D.F. Katz, S.A. Berger, Biorheology 17 (1980) 465.
[33] D.F. Katz, Am. J. Obstet. Gynecol. 165 (1991) 1984.
[34] K.G. Kornev, A.V. Neimark, J. Colloid Interface Sci. 235 (2001) 101.
[35] J. Szekely, A.W. Neumann, Y.K. Chuang, J. Colloid Interface Sci. 35 (1971) 273.
[36] E. Lorenceau, D. Quere, J.Y. Ollitrault, C. Clanet, Phys. Fluids 14 (2002) 1985.
[37] Y.M. Bajenov, Technology of Concrete, Vysshaya Shkola, Moscow, 1978.
[38] L.I. Kheifets, A.V. Neimark, Multiphase Processes in Porous Media, Khimia, Moscow, 1982.
[39] G.A. Akselrud, M.A. Altshuler, Introduction Capillary Chemical Technology, Khimia, Moscow, 1983.
[40] N. Ichikawa, Y. Satoda, J. Colloid Interface Sci. 162 (1994) 350.
[41] D. Quere, Europhys. Lett. 39 (1997) 533.
[42] J. Schoelkopf, P.A.C. Gane, C.J. Ridgway, G.P. Matthews, Nord. Pulp Paper Res. J. 15 (2000) 422.
[43] G. Vlastos, D. Lerche, B. Koch, O. Samba, M. Pohl, Rheol. Acta 36 (1997) 160.
[44] A.W. Adamson, A.P. Gast, Physical Chemistry of Surfaces, 6th ed., Wiley, New York, 1997.
[45] S. Middleman, Modeling Axisymmetric Flows: Dynamics of Films, Jets, and Drops, Academic Press, New York, 1995.
[46] M. Hanss, Biorheology 20 (1983) 199.
[47] G.B. Nash, J.G. Jones, J. Mikita, J.A. Dormandy, Clin. Hemorheol. 7 (1987) 482.
[48] J. Prothero, A.C. Burton, Biophys. J. 1 (1961) 565.
[49] M.J. Lighthil, J. Fluid Mech. 34 (1968) 113.
[50] J.M. Fitz-Gerald, Proc. R. Soc. London Ser. B 174 (1969) 193.
[51] J.M. Fitz-Gerald, J. Fluid Mech. 51 (1972) 463.
[52] P.J. Abatti, IEEE Trans. Biomed. Eng. 44 (1997) 209.
[53] P.G. de Gennes, Scaling Concepts in Polymer Physics, Cornell Univ. Press, New York, 1979.
[54] E.A. Evans, R. Skalak, Mechanics and Thermodynamics of Biomembranes, CRC Press, Boca Raton, FL, 1980.
[55] D. Needham, MRS Bull. 24 (1999) 32.
[56] R.M. Hochmuth, N. Mohandas, P.L. Blackshe, Biophys. J. 13 (1973) 747.
[57] E.A. Evans, Biophys. J. 13 (1973) 941.

[58] H.L. Goldsmith, in: D.A. Siginer, D. DeKee, R.P. Chhabra (Eds.), Advances in the Flow and Rheology of Non-Newtonian Fluids, Vol. A, Elsevier, New York, 1999, p. 1.
[59] T. Hasegawa, T. Iwaida, J. Non-Newtonian Fluid Mech. 15 (1984) 257.
[60] T. Hasegawa, T. Iwaida, J. Non-Newtonian Fluid Mech. 15 (1984) 279.
[61] J.Y. Yoo, M. Ahrens, D.D. Joseph, J. Fluid Mech. 153 (1985) 203.
[62] M.A. Brutyan, P.L. Krapivsky, Adv. Sci. Technol. VINITY 4 (1991) 3.